IEEE Access
Multidisciplinary | Rapid Review | Open Access Journal

Received March 22, 2020, accepted April 13, 2020, date of publication April 28, 2020, date of current version May 14, 2020.

Digital Object Identifier 10.1109/ACCESS.2020.2990922

Surface Roughness Detection of Roof Insulator Based on Hyperspectral Technology

CHAOQUN SHI[1], HAOLUN ZENG[2], YUJUN GUO[1], (Member, IEEE), KAI LIU[1], XUEQIN ZHANG[1], (Member, IEEE), AND GUANGNING WU[1], (Fellow, IEEE)

[1]School of Electrical Engineering, Southwest Jiaotong University, Chengdu 610031, China
[2]Chengdu Metro Media Company, Ltd., Chengdu 610041, China

Corresponding author: Yujun Guo (yjguo@swjtu.edu.cn)

This work was supported in part by the National Natural Science Foundation of China under Grant 51507146 and Grant 51325704, and in part by the Special Funds of Basic Scientific Research for Central University of the Ministry of Education of China under Grant 2682016ZDPY05.

ABSTRACT The strong airflow generated during the operation of the high-speed train will carry sand and dust, causing high-speed sand and dust to hit the surface of the external equipment of the vehicle body, which will increase the surface roughness of the roof insulators, resulting in the changes of the hydrophobicity, fouling characteristics and insulation performance of the insulator. It poses a hidden danger to the safe and stable operation of the train. In our existing surface roughness testing methods, contact detections and optical stylus methods can cause damage to the insulator surface. Infrared detection methods will be disturbed by leakage current. Most methods need to be disassembled for testing. These methods have certain disadvantages. Therefore, this paper proposes a non-contact detection method for the surface roughness of the roof insulators. Firstly, we extract the image information of the insulator surface by hyperspectral imager, then preprocess the extracted hyperspectral image and use the continuous projection algorithm to reduce the data. Finally, we use the support vector machine to construct the insulator surface roughness discriminant model, and successfully realize the hyperspectral detection method of the surface roughness of the roof insulators, and verify the effectiveness of the proposed method by experiments. As a non-contact detection method, this method can detect the surface roughness of the roof insulators in the non-disassembly conditions, and help the field staffs to grasp the surface roughness of the high-speed train roof insulators in time.

INDEX TERMS Roof insulator, surface roughness, hyperspectral technology, non-contact detection, support vector machines.

I. INTRODUCTION

As important high-voltage insulation components, the roof insulators serve to support the pantograph and isolate the train body in the high-speed railway [1]–[5]. Taking the Lanxin line as an example, when the high-speed train runs in the strong sandstorm area, a large amount of sand and dust carried in the air will hit the surface of the external equipment of the high-speed train at high speed. Due to the relative movement of high-speed trains and sand, the average relative speed of trains and sand can reach 110 m/s, which causes abrasion damages on the surface of the roof insulators. Therefore, as the trains running time increases, the surface roughness of the insulators will gradually increase [6], [7]. The changes of the surface roughness on the insulators directly cause the transformations and deterioration of their hydrophobicity, fouling characteristics and flashover characteristics, which will result in safety hazards in the driving [8].

At present, the detections of surface roughness on high-speed railway insulators are mainly divided into contact measurement and non-contact measurement. Most of them are unloaded in the laboratories or on sites for off-line inspections. Among them, contact measurements usually use needle touch methods. The drawback is that it is not possible to perform on-line detections under live conditions, and they have scratch damages to the high-precision surfaces and the soft material surfaces. And non-contact measurement methods mainly adopt infrared spectroscopy and optical stylus for detections. The optical stylus method uses laser to detect, which will cause slight damages on the insulators surface to

The associate editor coordinating the review of this manuscript and approving it for publication was Yongqiang Zhao.

a certain extent [9], and is not suitable for insulators still in service. The principle of detections by infrared spectroscopy is mainly based on the changes of thermal infrared radiation characteristics caused by the surface roughness of the material. Kaushal Verma *et al.* developed the Fizeau infrared interferometer to measure the thermal deformation of the surface of rough electronic components [10], He Jun *et al.* used infrared interference technology to detect the roughness of large caliber spherical surface [11], Li Zongnan *et al.* used infrared structured light technology to measure the surface roughness of soil [12]. The surface roughness of insulators of high-speed trains are detected by infrared spectrum methods, which cannot eliminate the influence of heat generated by leakage current during operation, and still cannot realize online monitoring. Therefore, it is important to pro-pose a surface roughness online test method that can perform on site.

Hyperspectral technology can continuously image the target object in tens or hundreds of spectral bands within its spectral coverage and obtain spectral information with uniform spectrum, which has the characteristics of large amount of information and high recognition. At present, insulators detection methods based on hyperspectral technology are mainly used in insulators aging, contamination and efflorescence detections [13]–[15]. In this paper, hyperspectral imager is proposed to extract the insulators surface image information, the extracted map data was processed and modeled, and the surface roughness grade discrimination model of insulators was constructed to realize the surface roughness detection of roof insulators based on hyperspectral technology, and the effectiveness of the proposed method was verified by experiments.

II. THEORETICAL BASIS

A. HYPERSPECTRAL IMAGING

Hyperspectral imaging technology is based on a lot of narrow band image data technology. It combines imaging technology and spectral technology to detect the two-dimensional geometric space and one-dimensional spectral information of the target and obtain the continuous and narrow band image data of hyperspectral resolution. Presently, hyperspectral imaging technology has developed rapidly, including grating splitting, acousto-optic tunable filtering splitting, prism splitting, chip coating and so on. It can be used in food safety, medical diagnosis, aerospace and other fields [16].

The key technologies of hyperspectral imaging include image acquisition, transmission and processing. Among them, spectral radiation, calibration and spectral information processing of imaging spectrometer are the main contents to realize spectral imaging. The main purpose of spectral imaging is to decompose the energy entering the detector into electromagnetic waves of different wavelengths, including the dispersion and interference method. Since the dispersion method appears very early, the technology is relatively mature but the imaging effect is not very satisfactory. In comparison, the effect of time modulation interferometric imaging mode is much better, which it can get the spectrum of different wavelength according to the interferogram of different optical path. The time modulation process can be realized via the Fourier transform.

Suppose the incident light generated from the light source is a perfectly collimated monochromatic beam with an amplitude α in complex number and the wave number is σ. When it is transmitted to an ideal lossless beam splitter, it is assumed that the reflectance and the projection ratio of the beam splitter are r, t, respectively. In this way, the incident light is divided into the reflected light αr and αt. After passing through plane mirror 1 and plane mirror 2, as is shown in Fig. 1, the two beams of light return to the splitter, and form two coherent beams after passing through the beam splitter, which are received by the detector, and the received signal amplitude is:

$$A = rt\alpha + rt\alpha e^{-i\varphi} \tag{1}$$

where φ is the phase difference.

The first and the second item in (1) stand for the longitudinal beam and the transverse beam, respectively. The signal intensity of interference light can be described using (2).

$$I_D(x,\sigma) = AA^* = 2RTB_0(\sigma)(1+\cos\varphi) \tag{2}$$

with

$$\varphi = 2\pi\sigma x$$

where x is the optical path difference, constant R and T represent the reflectance and projection ratio, respectively. $B_0(\sigma)$ is the intensity of the input light beam.

The general expression of interferogram can thus be obtained by integrating all wave numbers:

$$I_D(x) = \int dI_D(x,\sigma) = \int_0^\infty 2RTB_0(\sigma)[1+\cos(2\pi\sigma x)]d\sigma \tag{3}$$

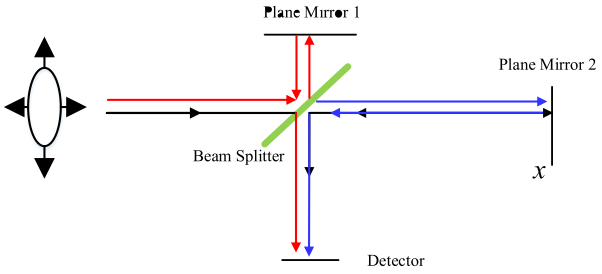

FIGURE 1. The principle of interferogram generating spectrogram.

This is equivalent to all the energy received by the detector at a certain position x at the mirror 2 of the interferometer in Fig. 1. When ignore the DC signals from (3), the general expression for interferogram become:

$$I_D(x) = C\int_0^\infty RTB_0(\sigma)\cos(2\pi\sigma x)d\sigma \tag{4}$$

with C stands for a constant.

Then, equation (4) can be expanded to plural form:

$$I_D(x) = \int_{-\infty}^{+\infty} RTB_0(\sigma) e^{i2\pi\sigma x} d\sigma,$$
$$I_D(x) \overset{\text{Fourier transform pair}}{\longleftrightarrow} RTB_0(\sigma) \quad (5)$$

Finally, the spectrogram can be obtained and represented using (6).

$$RTB_0(\sigma) = \int_{-\infty}^{+\infty} I_D(x) e^{i2\pi\sigma x} dx = FT^{-1}[I_D(x)] \quad (6)$$

where $F(\cdot)$ is the Fourier transform.

B. THEORY OF HYPERSPECTRAL BASED SURFACE ROUGHNESS DETECTION

In related researches, the main principle of the detection methods with hyperspectral technology is to detect different spectral absorption and reflection characteristics of different substances. Reflected on the hyperspectral images, the substances of different substances or different contents have different map information, and there are obvious differences in some characteristic bands. The essence is that the reflectance changes.

When the incident light is irradiated to the surface of the object, part of the light is absorbed by the material, and the other part of the light forms specular is reflected and show diffuse reflection according to the surface roughness of the object causing scattering. The scattered light intensity in the non-mirror direction corresponds to the surface roughness of the object in a certain range, as shown in Fig. 2. The conventional optical scattering method measures the surface roughness by measuring the distribution and ratio of scattered light and reflected light when a light illuminates to the surface [17].

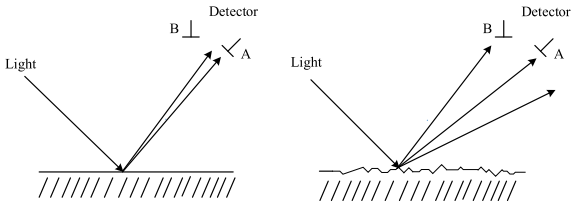

FIGURE 2. Schematic diagram of surface roughness detection by optical scattering method.

Hyperspectral imager is used to vertically extract the hyperspectral image of the target object. The hyperspectral imager is in the vertical direction of the target object to be tested. At this time, the scattered light intensity due to different surface roughness of the same object at the hyperspectral imager is different, resulting in different hyperspectral images, as shown in Fig.3.

Researches show that there is a certain degree of correlation between the surface roughness and the scattered light intensity distribution. Less surface roughness has stronger reflection and weaker scattering, while larger surface roughness has weaker reflection and stronger scattering [18].

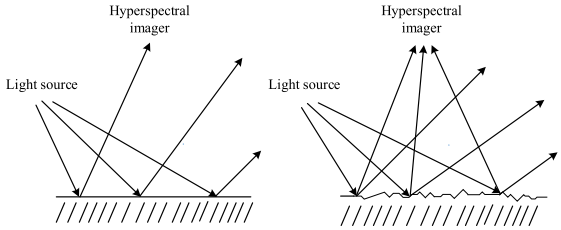

FIGURE 3. Schematic diagram of hyperspectral surface roughness detection.

Therefore, when a hyperspectral imager is used to acquire a hyperspectral image of a target object, as the surface roughness increases, the intensity of the scattered light received at the position of the hyperspectral imager increases, resulting in an increase in the reflectance of the target object. While the composition of the target object does not change, the hyperspectral line waveform does not change and the overall amplitude gradually increases. For the processing and modeling of the hyperspectral spectral line, hyperspectral detection of the insulator surface roughness degree can be detected.

III. EXPERIMENT AND MEASUREMENT

A. EXPERIMENTAL SAMPLE PREPARATION

In this paper, the insulator samples were prepared by sandpaper grinding method, and the roughness of the prepared insulator samples were measured by a traditional stylus surface roughness measuring instrument. Therefore, the influence of the amount of grit in the sandpaper on the surface roughness of the insulators can be ignored. Considering that during the operation of high speed trains, the direction of high-speed sand and dust is opposite to that of the trains, and strip-shaped abrasion marks will be formed on the surface of the insulators. Therefore, when preparing samples, it is necessary to polish the samples in the same direction with sandpaper to form horizontal strip abrasion marks.

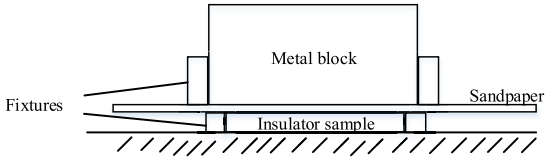

FIGURE 4. Schematic diagram of test sample preparation.

As shown in Fig. 4, a good insulator sample of 5 cm × 5 cm was selected and fixed on the table to ensure that the sample did not slip during the grinding process. The insulator samples were polished with 240 mesh sandpaper. A square anvil with a volume of 72 mm × 72 cm × 30 mm and a weight of about 1.31 kg was placed over the insulator sample, and it was fixed by a fixing device to ensure that it did not slip during the grinding process. In this way, it was ensured that the pressure applied in the vertical direction of the sandpaper was the same in each polishing processes.

Each time sandpaper moved 40 cm horizontally to complete one polishing process.

B. SURFACE ROUGHNESS TEST

The surface roughness of the polished insulator samples were detected by the stylus type surface roughness test method. Use HOMMEL-ETAMIC T8000RC-400 Digital roughness measuring instrument, the measured value is Ra(Arithmetic mean deviation). Five points were measured on the surface of each insulator samples, and the results were aver-aged. The insulator samples with 0, 5, 10, 15 and 30 times of grinding were selected for testing. The sample is shown in Fig. 5. The results are shown in Tab. 1.

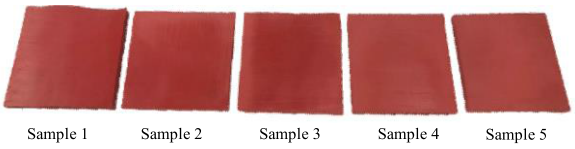

FIGURE 5. Insulator sample diagram.

TABLE 1. Surface roughness measurement data of the sample.

Sample number	Ra (μm)					Average value (μm)
1	0.86	0.82	0.84	0.82	0.85	0.84
2	2.31	2.43	2.77	2.47	2.63	2.52
3	3.29	2.75	3.14	3.01	2.96	3.03
4	3.35	2.87	3.13	3.79	3.41	3.31
5	3.77	3.64	3.79	3.35	3.83	3.68

Samples 1 to 5 were insulator samples that were unpolished, polished 5 times, polished 10 times, polished 15 times, and polished 30 times. During the grinding process, it was found that the surface rough-ness of the insulators tended to be stable after grinding for about 30 times, and the surface roughness of the samples no longer increased significantly with the increasing times of polishing. Therefore, the insulator samples was divided into 1 to 5 levels by grading with these 5 roughness.

C. HYPERSPECTRAL IMAGE DETECTION PLATFORM

This article used the hyperspectral imager GaiaField-F-V10, standard proofreading whiteboard and fill light to build an insulator hyperspectral image detection platform. The hyperspectral imager has a spectral range of 400-1000 nm and a spectral resolution of 3.8 nm, a total of 256 bands. The hyperspectral imager is located in the vertical plane in the middle of the test platform, obliquely downward 45°, 120 cm away from the test platform. The acquired hyperspectral image is directly transmitted to the computer through the USB cable, as shown in Fig. 6.

The fill light was used to meet the inspection requirements. The samples are placed adjacent to the standard calibration whiteboard and at the same plane on the inspection platform.

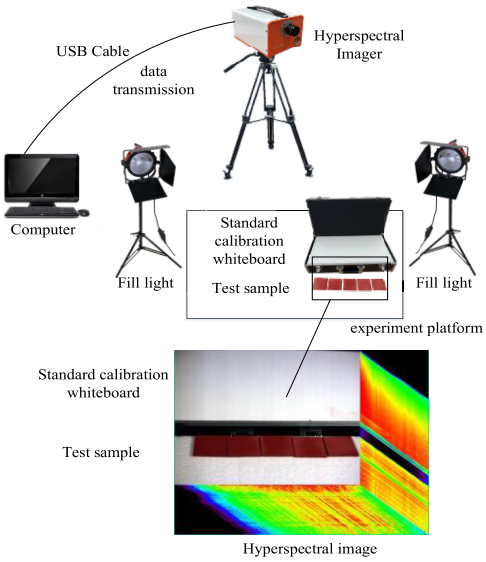

FIGURE 6. Hyperspectral image detection platform.

The hyperspectral imager was used to extract the hyperspectral images of the samples and the standard calibration whiteboard. And the obtained hyperspectral images are uploaded to the computer.

For the insulator samples of the five different roughness grades, 50 regions with an extraction area of not more than 1 mm × 1 mm were randomly and non-repeated extracted and 50 hyperspectral spectral lines corresponding to these regions were obtained as training samples. In addition, 20 regions of the extraction area of not more than 1 mm × 1 mm were randomly and non-repeated selected and 20 hyper-spectral spectral lines corresponding to these regions were obtained as test samples. A total of 250 lines were obtained as training samples, and 100 lines were used as test samples. The obtained hyperspectral images were converted into tabular data storage, and subsequent data processing and modeling were per-formed.

IV. HYPERSPECTRAL IMAGE DATA PROCESSING

A. HYPERSPECTRAL IMAGE PREPROCESSING

The black-and-white correction of the acquired hyperspectral images through the standard calibration whiteboard can make the reflectance of the sample obtained under different illumination conditions consistent, thus overcoming the experimental error caused by the difference of the illumination intensity to some extent. The black-and-white correction algorithm is as follows:

$$R(\%) = \frac{R_0 - D}{W - D} \times 100\% \tag{7}$$

where R is the corrected reflection spectrum image data, R_0 is the original reflection spectrum image data of the sample, D is the reflection image data of the standard blackboard, and W is the reflection image data of the standard whiteboard.

The hyperspectral images of the 5 mm × 5 mm region at the center of the insulator samples in Fig. 5 were extracted, and the hyperspectral lines were calculated and processed by black and white correction. The results are shown in Fig. 7.

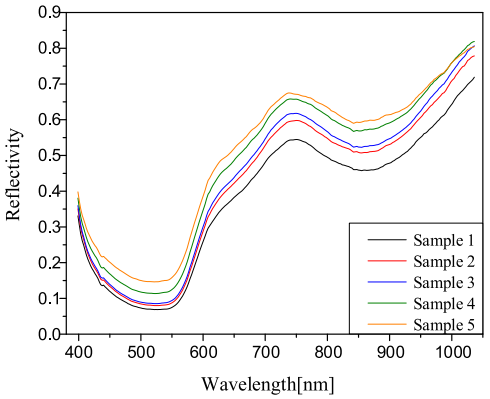

FIGURE 7. Hyperspectral line graph of the center of the sample after black and white correction.

To a certain extent, as the surface roughness of the insulator samples 1 to 5 gradually increases, the overall spectral lines of the hyperspectral line images in the central region tend to be similar but the overall reflectance show an upward trend. In order to avoid the contingency of the data and verify the effectiveness of the method, this paper selected a large amount of data for modeling. The obtained 250 training sample lines and 100 test sample lines were processed by black and white correction method. The corrected training sample lines are shown in Fig. 8.

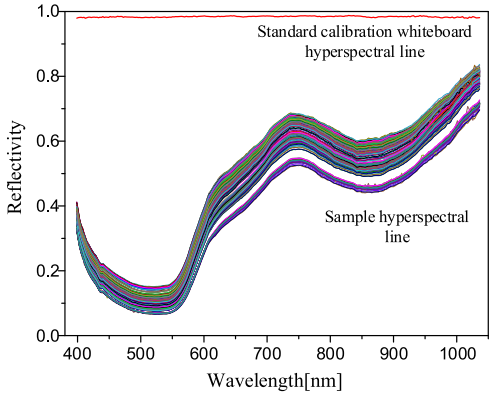

FIGURE 8. Hyperspectral line graph of black and white corrected training samples.

B. FEATURE SPECTRAL BANDS EXTRACTION

The image information extracted by hyperspectral technology has the disadvantage of a large amount of data which has a large amount of redundant information. Therefore, in order to improve the recognition rate, classification accuracy and algorithm operation speed of hyperspectral images, it is necessary to select a combination of bands with large amount of effective information, small correlation, and class separability to complete data dimensionality reduction.

For the insulator surface roughness grade discrination model proposed in this paper, the main parameter is the reflectivity corresponding to certain wavelength. In this paper, the successive projections algorithm is used to extract the feature spectral bands. The successive projection algorithm can effectively eliminate the redundant information in the original spectral matrix and filter out the optimal spectral bands with respect to the target information. The successive projection algorithm is as follows [19].

Take $x_{k(0)}$ and N as the initial iteration vectors and the number of feature variables to be extracted, respectively, and the spectral matrix dimension is J. When starting a new calculation, randomly select a column j, assign x_j, denoted as $x_{k(0)}$, and record the rest of the remaining column vector positions as s; $s = \{j, 1 \le j \le \mathrm{J}, j \notin \{k(0), \ldots, k(n-1)\}\}$; calculate the projection of x_j to the variables in s:

$$P_{x_j} = x_j - (x_j^T x_{k(n-1)})(x_{k(n-1)}^T x_{k(n-1)})^{-1}, \quad j \in s \tag{8}$$

Take $k(n) = \arg(\max(\|Px_j\|), j \in s)$; take $x_j = Px_j, j \in s$; $n = n+1$, if $n < N$, return to step (2) for calculation. Finally, multiple linear regression is performed on each pair of $x_{k(0)}$ and N obtained by calculation, and $x_{k(0)}$ and N with the smallest mean standard deviation are selected as the optimal solution.

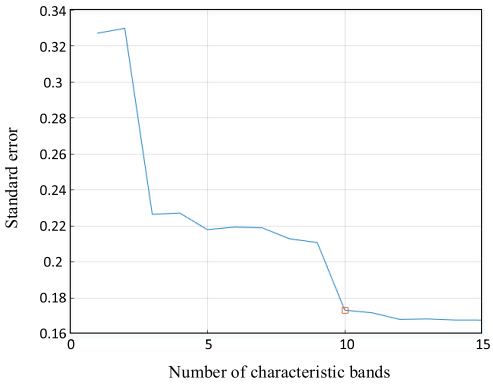

FIGURE 9. Selection diagram of the number of feature bands and standard error.

The training samples are processed by successive projection algorithm, and the obtained results are shown in Fig. 9 and Fig. 10. After considering the number of characteristic spectral bands and the standard error, take 10 characteristic spectral bands, and the standard deviation is 0.1734. The characteristic spectral bands are located in the full spectral bands at 2, 52, 141, 183, 243, 250, 251, 253, 255, and 256, respectively.

V. INSULATOR SURFACE ROUGHNESS GRADE DISCRINATION MODEL

A. SUPPORT VECTOR MACHINE

In this paper, the support vector machine is used to establish the insulator surface roughness grade discrimination model to

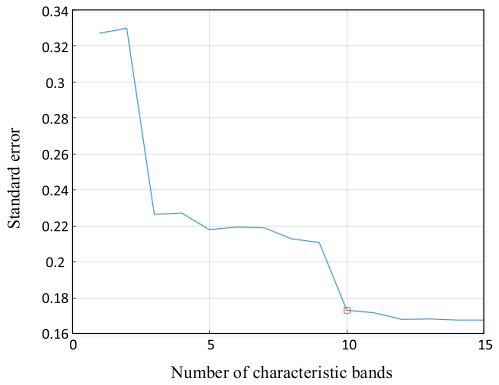

FIGURE 10. The position of the feature bands.

classify and predict the surface roughness of insulators [20]. As a machine learning algorithm based on statistical learning theory, SVM algorithm can transform low-dimensional input samples into high-dimensional samples for processing, so that samples in low-dimensional inseparability can be divisible in high-dimensional. At the same time, support vector machines are better than traditional maximum likelihood method, artificial neural network and other machine learning algorithms [21] in terms of small samples learning, anti-noise performance and learning efficiency.

For linearly separable training samples (x_i, y_i), $i = 1, 2, 3, \cdots, n, x_i \in \mathrm{R}^n$, n represents the number of data, x_i represents data points, y_i represents classified sample labels. In this case, in the d-dimensional data space, there is a hyperplane equation with respect to the deviation value b and the weight coefficient w:

$$f(x) = w^T x_i + b \tag{9}$$

For the linear indivisible problem in low latitude space, it can be transformed into a linear separable problem in high latitude space by nonlinear transformation. At this time, it is necessary to introduce a slack variable $\xi_i(\xi_i \geqslant 0)$ to obtain the optimal classification hyperplane optimization problem under the condition of linear inseparable condition:

$$\begin{aligned} &\min\ \Phi(w, \xi) = \frac{1}{2}\|w\|^2 + c\sum_{i=1}^{1}\xi_i \\ &\text{S.t. } y_i[(w \cdot x_i + b)] \geq 1 - \xi_i \end{aligned} \tag{10}$$

In the SVM classification model, the main parameters are the kernel function K and the punishment coefficient c. As this paper selects the RBF function as the kernel function, the kernel parameter that determines the distribution of data mapped to a new feature space is another key parameter needs to be determined. Parameter c is used to adjust the degree of punishment of the model for the right and wrong classification of the sample. The larger the value of c is, the smaller the model misclassification error is, that is, the smaller the tolerance to the error is, the over-fitting is easy to occur; the smaller degree of c is, the larger obtained model classification interval is, which has better generalization performance, but when c approaches 0, it will cause the algorithm to not converge, resulting in over-fitting. To solve this problem, the Lagrangian function is used to transform the equation (4):

$$L(w, b, \alpha) = \frac{1}{2}\|w\|^2 - \sum_{i=1}^{n}\alpha_i(y_i(w^T x_i + b) - 1 - \xi_i) \tag{11}$$

where α_i is the Lagrangian coefficient, $\alpha_i \leq c$, then the optimization function:

$$L(w, b, \alpha) = \sum_{i=1}^{n}\alpha_i - \frac{1}{2}\sum_{i,j=1}^{n}\alpha_i\alpha_j y_i y_j x^T x_j \tag{12}$$

The SVM introduces a kernel function to perform dimensional transformation. As long as a kernel function $K = (x_i, x_j)$ satisfies the Mercer conditions, the inner product in the corresponding transformation space can be obtained. Therefore, the high dimensional spatial linear classification of low-latitude spatial nonlinear problems can be realized by using the appropriate inner product function $K = (x_i, x_j)$. In this paper, the radial basis (RBF) kernel function is used for modeling. The RBF function is:

$$K(x_i, x_j) = \exp(-\|x_i - x_j\|^2/2\sigma^2) \tag{13}$$

At this point, the corresponding discriminant function is:

$$f(x) = \mathrm{sgn}\left(\sum_{i,j=1}^{n}\alpha_i y_i K(x_i \cot x_j) + b\right) \tag{14}$$

In this paper, the cross-validation method is used to optimize the penalty parameter c and the kernel parameter g, and the obtained modeling data is used to calculate the optimal c and g of the classification model.

The feature bands obtained by the successive projections algorithm were selected as the input variable corresponding to the processed hyperspectral image data, and the RBF kernel function was used for modeling. Modeling is performed without correcting the penalty parameter c and the kernel parameter g. At this time, the default value penalty parameter c is 2, the kernel parameter g is 1, and the operation result is as shown in Fig. 11.

The best accuracy calculated at this time is 91.91%, the accuracy of the test using the test samples is 91%, and 91 samples from 100 samples are accurately graded.

B. PARAMETRIC CROSS VALIDATION

Cross validation is mainly used in modeling applications. The purpose is to make the model obtained by training have a good fit to the data outside the training data by selecting the model with the best generalization performance. The main idea is to extract most of the samples in the training sample as the training set, a small part of the sample as the test set, train the model with the training set, and test the model obtained with the test set, and loop this step until all the data samples are tested only once as a test set to get the most accurate and stable model [22].

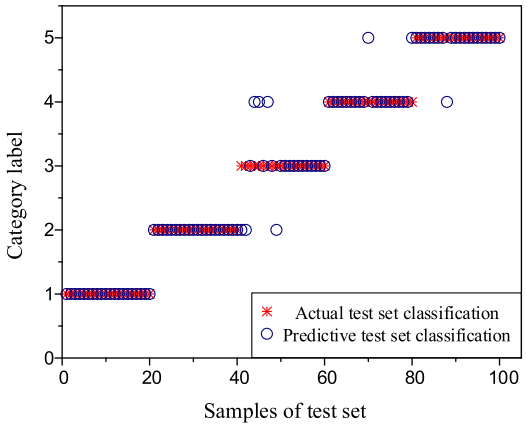

FIGURE 11. Calculation results without parameter correction.

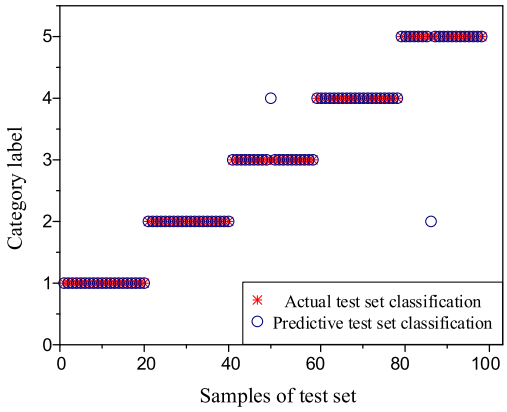

FIGURE 13. Calculation results after parameter correction.

In this paper, the cross-validation method is used to correct the penalty parameter c and the kernel parameter g of the support vector machine, so as to obtain the model with the best classification accuracy and stability.

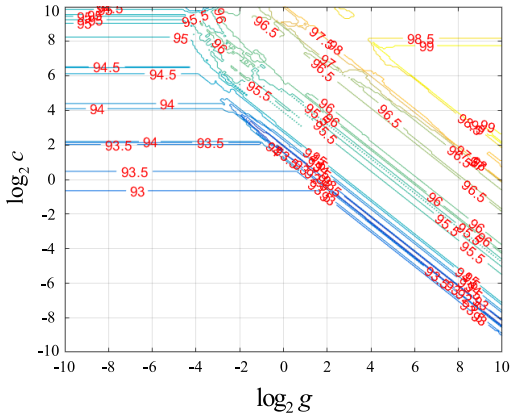

FIGURE 12. Selection chart of penalty parameter c and kernel parameter g.

As shown in Fig. 12, the x-axis is log2c and the y-axis is log2g. As the penalty parameter c and the kernel parameter g change, the accuracy of the model will change continuously, but the same accuracy may correspond to different combination of value c and g value. Therefore, in order to avoid excessive fitting of the penalty parameter c, we select the highest accuracy, but the minimum value of c and g is the optimal solution. At this time, the penalty parameter c is taken as 17.1484, and the value of the kernel parameter g is 238.8564, in the case of this combination of parameters, the accuracy of the model obtained by training the training samples is 97.06%.

As shown in Fig. 13, the penalty parameter c and the kernel parameter g obtained after the parameter correction are used to establish the surface roughness discrimination model of the insulator. The accuracy of the test using the test samples is 98%, 98 samples from 100 samples are accurately graded. Parameter correction can effectively improve the accuracy of the support vector machine model.

C. VALIDATION WITH FIELD COLLECTED DATA

For further validation, the real hyperspectral data collected from a roof insulator installed on the top of EMU is utilized for study. This insulator has been installed for 27 months since its first operation, and been cleaned four times per week. The insulator and corresponding hyperspectral lines for case study is given in Fig 14.

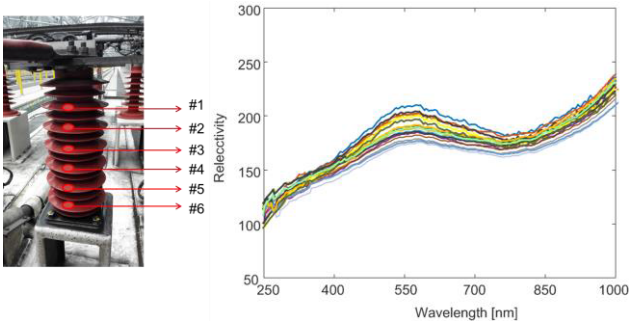

FIGURE 14. The insulator and corresponding hyperspectral lines for case study.

For the EMU roof insulator, six locations are selected to carry out the hyperspectral test, as shown in Fig. 14, each test location are repeated for 10 times and finally, 60 samples are collected. Test results of surface roughness is given in Table 2. The obtained spectral lines are preprocessed using the continuous projection method introduced in this paper and seven feature spectrum segments are extracted. They are 272.6nm, 458.1nm, 552.8nm, 574.6nm, 755.5nm, 889.4nm.

Once again, the SVM classification model is utilized for validation, 40 samples are used for SVM training while the remaining 20 samples are taken as test datasets. The value of penalty parameter c is also set to 2 and the kernel parameter g is set to unit. The training and test result are 92.5% and 90%, respectively. Obviously, the reflectivity-wavelength

TABLE 2. Surface roughness measurement data of the sample.

Sample location	Ra (μm)					Average value (μm)
1	0.84	0.81	0.85	0.79	0.81	0.82
2	1.23	1.26	1.29	1.27	1.25	1.26
3	2.35	2.31	2.26	2.28	2.3	2.30
4	2.85	2.88	2.96	2.95	2.99	2.93
5	2.58	2.63	2.45	2.66	2.53	2.57
6	1.58	1.55	1.49	1.63	1.52	1.55

pairs selected are effective for characterization of surface roughness.

VI. CONCLUSION

In this paper, the surface of the insulators was treated by sandpaper grinding method, and the roughness of the samples were measured and graded by the traditional contact roughness measurement method. Hyperspectral imager was used to obtain the hyperspectral images of the sample surface. The obtained image data was pre-processed and the insulator surface roughness discrimination model was established. The surface roughness detection method based on hyperspectral technology was proposed. The conclusions obtained are as follows:

1) The hyperspectral image lines of insulators with different surface roughness have a similar waveform and gradually increasing full-bands amplitude with the increase of the surface roughness of the insulator to a certain degree.

2) Using the vector machine to determine the surface roughness grade of the insulators after the parameter correction, the best accuracy rate of the model is 97.06%. The accuracy of the test with the actual test samples is 98%, which verifies the feasibility and effectiveness of using the hyperspectral technique to detect the surface roughness of the roof insulator.

3) The surface roughness detection method of roof insulator based on hyperspectral technology proposed in this paper can realize on-line detection of surface roughness of roof insulator, and has good application potential in surface roughness detection of roof insulator in non-disassembly condition.

REFERENCES

[1] X. Zhang, S. Peng, and G. Wu, "Cause of fog flashover on roof insulator and suppression effect of hot air flow," *High Voltage Eng.*, vol. 42, no. 11, pp. 3585–3592, 2016.
[2] G. Wu, C. Shi, and X. Zhang, "Research progress of roof insulator used for high-speed train," *Southern Power Syst. Technol.*, vol. 10, no. 3, pp. 71–77, 2016.
[3] X. Kong and M. Yang, "Influence of pantograph subsidence on high-speed train aerodynamic drag," *J. Railway Sci. Eng.*, vol. 14, no. 9, pp. 1805–1813, 2017.
[4] X. Chen, B. Cao, and Y. Liu, "Dynamic model of pantograph-catenary arc of train in high speed airflow field," *High Voltage Eng.*, vol. 42, no. 11, pp. 3593–3600, 2016.
[5] J. Sun, G. Wu, and W. Chen, "Dynamic simulation analysis of bar insulator pollution in strong wind," *J. Southwest Jiaotong Univ.*, vol. 47, no. 3, pp. 413–419, 2012.
[6] H. Luo, K. Liu, J. Ran, Y. Yue, X. Wang, S. Yap, and C. S. Wong, "Study of dielectric barrier Townsend discharge in 3-mm air gap at atmospheric pressure," *IEEE Trans. Plasma Sci.*, vol. 42, no. 5, pp. 1211–1215, May 2014.
[7] J. Sun, G. Gao, L. Zhou, and G. Wu, "Pollution accumulation on rail insulator in high-speed aerosol," *IEEE Trans. Dielectr. Electr. Insul.*, vol. 20, no. 3, pp. 731–738, Jun. 2013.
[8] L. Cheng, H. Qian, and Z. Wang, "Study on Abradability of silicone rubber at high speed," *Silicone Mater.*, no. 6, pp. 440–443, 2014.
[9] B. Guo, "An overview of the research on surface roughness measuring method," *Value Eng.*, vol. 30, no. 8, pp. 50–51, 2011.
[10] K. Verma and B. Han, "Far-infrared Fizeau interferometry," *Appl. Opt.*, vol. 40, no. 28, pp. 4981–4987, Oct. 2001.
[11] H. Jun, L. Chen, and X. Li, "Measurement of large aperture rough sphere," *J. Appl. Opt.*, vol. 30, no. 6, pp. 969–973, 2009.
[12] Z. Li, Z. Chen, L. Wang, and Z. Jiang, "A measuring method of soil surface roughness using infrared structured light 3D technology," *Trans. Chin. Soc. Agricult. Eng.*, vol. 29, no. 21, pp. 137–142, 2013.
[13] Z. Wen, C. Kong, and X. Min, "Working state detection of composite insulator by hyperspectral remote sensing," *High Voltage App.*, no. 2, pp. 75–79, 2014.
[14] T. Xiang, X. Wang, and Y. Luo, "Research of composite insulator powder status non-contact detection technology," *China Electr. Power, Technol. Ed.*, no. 10, pp. 321–327, 2015.
[15] G. Shao, J. Fu, and Y. Chen, "Aging assessment method of composite insulator using neural network based on image and spectra characteristics," *High Voltage Eng.*, vol. 40, no. 3, pp. 457–465, 2014.
[16] Q. Tong, B. Zhang, L. Zheng. *Hyperspectral Remote Sensing*. Beijing, China: Higher Education Press, 2006, pp. 50–58.
[17] S. Zhou, "Fiber Optic surface roughness sensor," *Acta Photonica Sinica*, vol. 24, no. 2, 1995.
[18] C. Liu, R. Lu, and L. Chen, "Progress of surface roughness measurement based on optical method," *Semiconductor Optoelectron.*, vol. 31, no. 4, pp. 495–500, 2010.
[19] D. Wu, J. Ning, and X. Liu, "Determination of anthocyanin content in grape skins using hyperspectral imaging technique and successive projections algorithm," *Food Sci.*, vol. 35, no. 8, pp. 57–61, 2014.
[20] K. Tan, "Hyperspectral remote sensing image classification based on support vector machine," *J. Infr. Millim. Waves*, vol. 27, no. 2, pp. 123–128, Dec. 2008.
[21] W. Tian, D. He, and D. Yang, "A method for predicting TVB-N content of cooked beef based on hyperspectral image," *Food Machinery*, vol. 32, no. 12, pp. 70–74, 2016.
[22] G. Yang, X. Yu, and X. Zhou, "Research on relevance vector machine for hyperspectral imagery classification," *Acta Geodaetica et Cartographica Sinica*, vol. 39, no. 8, pp. 2029–2031, 2008.

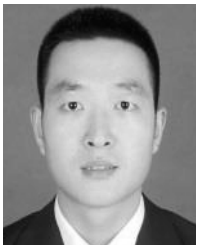

CHAOQUN SHI was born in Zhoukou, China, in 1989. He received the M.S. degree in electrical engineering from Southwest Jiaotong University, Chengdu, China, in 2014, where he is currently pursuing the Ph.D. degree in electrical engineering with the School of Electrical Engineering. His major research fields are outdoor insulation for high-speed railway and electrical discharge.

HAOLUN ZENG was born in Chengdu, China, in 1993. He received the M.Sc. degree in electrical engineering from Southwest Jiaotong University, Chengdu, China, in 2016. He is currently an Engineer with Chengdu Metro Media Company, Ltd. His research interests include external insulation protection and gas discharge.

YUJUN GUO (Member, IEEE) was born in Wuhan, China, in 1989. He received the B.Sc. degree in electrical engineering from the Huazhong University of Science and Technology, Wuhan, China, in 2011, and the Ph.D. degree in electrical engineering from Chongqing University, Chongqing, China, in 2017. He is currently a Lecturer with the School of Electrical Engineering, Southwest Jiaotong University. His research interests are outdoor insulation and protection of transmission lines.

KAI LIU was born in Guiyang, China, in 1990. He received the B.E. degree from the University of Electronic Science and Technology of China, Chengdu, China, in 2013, and the Ph.D. degree in electrical engineering from Chongqing University, Chongqing, China, in 2018. His current research interests include the fault diagnosis of grounding grid and the multiphysics coupling field calculation for power system device.

XUEQIN ZHANG (Member, IEEE) was born in Chengdu, China, in 1979. She received the B.Sc. and Ph.D. degrees in electrical engineering from Southwest Jiaotong University, Chengdu, China, in 2002 and 2008, respectively. She is currently an Associate Professor with the School of Electrical Engineering, Southwest Jiaotong University. Her research interest is high voltage and insulation technology.

GUANGNING WU (Fellow, IEEE) was born in Nanjing, China, in 1969. He received the B.Sc., M.Sc., and Ph.D. degrees in electrical engineering from Xi'an Jiaotong University, Xi'an, China, in 1991, 1994, and 1997, respectively. He is currently a Professor with the School of Electrical Engineering, Southwest Jiaotong University, Chengdu, China. His research interests include condition monitoring, fault diagnosis, and insulation life-span evaluation for electrical equipment.